

Anisotropy and Inhomogeneity in Drifter Dispersion

Helga S. Huntley¹, B. L. Lippardt, Jr.², and A. D. Kirwan, Jr.¹

¹School of Marine Science and Policy, University of Delaware, Newark, Delaware, USA.

²formerly: School of Marine Science and Policy, University of Delaware, Newark, Delaware, USA.

Key Points:

- Local anisotropy is observed across all scales in the initial evolution of pair separations.
- Averaged over multiple deployments, the observed local anisotropy tends to average out.
- Local inhomogeneity is observed in pair separation statistics for at least a week.

Corresponding author: H. S. Huntley, helgah@udel.edu

This article has been accepted for publication and undergone full peer review but has not been through the copyediting, typesetting, pagination and proofreading process which may lead to differences between this version and the Version of Record. Please cite this article as doi: 10.1029/2019JC015179

Abstract

Ocean flows are known to be locally anisotropic and inhomogeneous. Nonetheless, the ocean's statistical dispersion properties are traditionally assumed to be isotropic and homogeneous. Here, we investigate the effect of local anisotropy and inhomogeneity on dispersion statistics, using a unique dataset of roughly 300 near-surface drifters that were launched within 10 days in the summer of 2012. The unique launch strategy based on nested triplets resulted in an unusually large number of nearly co-located drifter pairs. Thus, this dataset is ideally suited for an estimate of the directional bias and inhomogeneity effects inherent in drifter-pair statistics.

Several metrics are proposed to assess the time evolution of anisotropy and inhomogeneity effects at multiple initial separation scales (100 m, 200 m, 500 m, 1 km, and 10 km). Locally, statistically significant anisotropy and inhomogeneity are observed at all scales, although anisotropy is noticeably less at 10 km, suggesting that the energetic processes driving anisotropic dispersion operate primarily at smaller scales. Moreover, averaged over a sufficient variety of different flow regimes, the signature of both anisotropy and inhomogeneity in dispersion metrics lessens. These trends hold generally across all scales, with longer time scales associated with larger spatial scales. The results indicate that oceanic dispersion is statistically isotropic and homogeneous over large swaths, but for an application in a specific location, local anisotropy and inhomogeneity matter. What size swath is large enough is situation-dependent: For this specific dataset, statistics had to be evaluated over multiple deployments, giving a required area greater than 150 km².

1 Introduction

With its many fronts, eddies, and jets, the ocean circulation is well known to be locally anisotropic and inhomogeneous. Yet the dispersion properties of the ocean have traditionally been studied in the context of isotropic homogeneous turbulence theory (Bennett, 1987; LaCasce, 2008). This requires assumptions of statistical isotropy and homogeneity, where averages are taken over space, time, or both. Applications to mesoscale and large-scale ($\geq O(100 \text{ km})$) phenomena in the ocean have required only modest theoretical extensions to differentiate the vastly different magnitudes of horizontal and vertical mixing (Kirwan, 1969). This paradigm has been successfully applied to describe the generally dispersive nature of the ocean. In the last few decades, as the understanding

and predictability of mesoscale and large-scale flows has matured, attention has turned to the role of the submesoscale (e.g., McWilliams, 2016). It has become increasingly clear that an energetic submesoscale flow field introduces local anisotropy and inhomogeneity (e.g., Lapeyre & Klein, 2006; Capet et al., 2008; Gula et al., 2014; Shulman et al., 2015), leading to local clustering of passive tracers in a statistically dispersive ocean (Huntley et al., 2015; Jacobs et al., 2016; D'Asaro et al., 2018). Anisotropy and inhomogeneity are likely stronger at the smaller scales, where the effects of frontogenetic processes are more prominent. But at some averaging scale, the transition must happen where statistical isotropy and homogeneity are realized. Here we seek to quantify the local anisotropy and inhomogeneity and how they impact dispersion estimates based necessarily on relatively sparse and strongly non-uniform samples.

With the wide-spread use of GPS-tracked surface drifters and sonar-tracked sub-surface floats, empirical dispersion estimates have proliferated. Early examples include studies in the eastern North Pacific (Kirwan et al., 1978) and off northern California (Davis, 1985). Several groups have explored the dispersion characteristics of the Northern Atlantic, using both sub-surface (LaCasce & Bower, 2000; Zhang et al., 2001; Ollitrault et al., 2005) and near-surface (Lumpkin & Eliot, 2010) drifters, of the Mediterranean Sea (Lacorata et al., 2001; Schroeder et al., 2011, 2012), and of the Gulf of Mexico (LaCasce & Ohlmann, 2003; Poje et al., 2014; Beron-Vera & LaCasce, 2016; Zavala Sansón et al., 2017). A handful of papers have looked at less well-studied areas, such as the Nordic Seas (Koszalka et al., 2009), the Gulf of Finland (Torsvik & Kalda, 2014), and the Great Barrier Reef region off Australia (Mantovanelli et al., 2012). Such regional studies implicitly acknowledge potential inhomogeneity at super-regional scales. On smaller scales, the limitations of homogeneous turbulence as a conceptual model for real ocean flows in the nearshore region have recently been highlighted by Spydell et al. (2019) based on idealized simulations. Anisotropy has also been identified as a potential issue: For example, LaCasce and Bower (2000), Berti et al. (2011), and Corrado et al. (2017) found anisotropic relative dispersion by separating individual pair separations into zonal and meridional or along- and cross-jet components. Anisotropic dispersion has also been observed in the deformation of drifter triplets (LaCasce & Ohlmann, 2003; Berta et al., 2016). Motivated by numerical studies that found anisotropic dispersion aligned with bathymetry (Romero et al., 2013) or wind (Mensa et al., 2015), Ohlmann et al. (2019) presented a first attempt to quantify anisotropy in drifter and dye patch observations along the coast of the west-

75 ern Gulf of Mexico. At scales of $O(100\text{ m})$, they found weak anisotropy in geographic
76 coordinates (along- and cross-shore), but strong anisotropy when using axes aligned with
77 maximum and minimum dispersion over two-hour intervals.

78 Expanding on these findings, we make use of the drifter data collected in summer
79 2012 by the Consortium for Advanced Research on Transport of Hydrocarbon in the En-
80 vironment (CARTHE) in the northern Gulf of Mexico during the Grand Lagrangian De-
81 ployment (GLAD, Poje et al., 2014). Hundreds of drifters were deployed within a small
82 time window and within a contained geographic area, targeting the submesoscale flows.
83 This dataset is particularly amenable to our analysis because drifters were released in
84 nested triangles. Each triangle provides three pairs at nearby locations with nearly iden-
85 tical initial spacing, but oriented differently, allowing for an investigation of the effects
86 of local anisotropy. By pairing one member of one triangle with a member of a second
87 triangle, any two triangles taken together provide nine pairs with similar initial spacing,
88 oriented in the same direction, but with slight modifications to the initial position. These
89 groups can be used to assess the impact of local inhomogeneity.

90 The plethora of original triplets in the GLAD dataset is also ideal to study the two-
91 dimensional dispersion and the patch deformation properties of the flow in the area. This
92 type of analysis was pioneered by LaCasce and Ohlmann (2003). At the time, they had
93 to rely on chance-triplets arising from the Surface Current and Lagrangian Drift Pro-
94 gram (SCULP) deployment of the mid-1990s, with separation scales on the order of kilo-
95 meters. The use of chance pairs can introduce biases into the statistics, as drifters over
96 time preferentially sample convergence regions (Haza et al., 2008). Using original GLAD
97 triangles, Berta et al. (2016) analyzed the shape deformations for two different initial
98 sizes, 100 m and 500 m nominal side length. Consistent with the coastal study by Ohlmann
99 et al. (2019), they found highly elongated configurations after relatively short time in-
100 tervals (6 hours to 2 days), much shorter than for comparable synthetic drifter triplets
101 advected in the geostrophic velocity field derived from satellite altimetry data (6 days).
102 The associated time scales were scale- and location-dependent. We place our results for
103 anisotropy and inhomogeneity effects on pair-wise, or one-dimensional, dispersion esti-
104 mates into the context of these findings of anisotropic and inhomogeneous two-dimensional
105 dispersion.

106 Our report is organized as follows: Section 2 describes the details of the drifter de-
107 sign and the deployment strategy (Section 2.1) and defines the metrics used to quantify
108 the anisotropy and inhomogeneity impacts (Section 2.2). Results on pair-separation statis-
109 tics are described in Section 3, followed by the comparison with triad statistics in Sec-
110 tion 4. We close with a discussion and conclusions in Section 5.

111 **2 Methods**

112 **2.1 Drifter data**

113 The drifters deployed during GLAD (Fig. 1a) were designed to measure ocean cur-
114 rents integrated over approximately the top 1 m, minimizing drag by wind and waves.
115 They largely emulated the design of the popular and much-tested CODE (Coastal Ocean
116 Dynamics Experiment) drifters from the 1980s (Davis, 1985) but were custom-built to
117 be cheap, making it affordable to deploy hundreds within a relatively small geographic
118 area. Each drifter was equipped with an off-the-shelf GPS unit reporting its position at
119 nominal 5-minute intervals with nominal position accuracy of 7 m (although recent tests
120 have shown position errors less than 2.5 m for 95% of records from similar units (Meyerjürgens
121 et al., 2019)). The original drifter launches took place between 20 July and 31 July 2012.
122 Roughly 80% of the drifters reported for more than one month, while 52% were still re-
123 porting after two months.

124 The raw position data were quality controlled by eliminating out-of-range values
125 for longitudes and latitudes. Records were ended when no positions were reported for
126 more than 24 consecutive hours, when the drifter was known to have been picked up, or
127 when such an “abduction” was suspected due to speeds exceeding an average of 1.85 m/s
128 over a 12-hour period. Individual position records were deleted if they implied a speed
129 in excess of 3 m/s for either adjacent interval or if they implied a rotation greater than
130 360 degrees within three hours. Further outliers were identified by comparing positions
131 to estimated positions from a spline fit using neighboring points. These were removed
132 if differences greater than 100 m were found. The remaining data points were consid-
133 ered valid and spline-interpolated to uniform five-minute time points. See Yaremchuk
134 and Coelho (2015) for further details. This processed dataset is publicly available (Özgökmen,
135 2013).

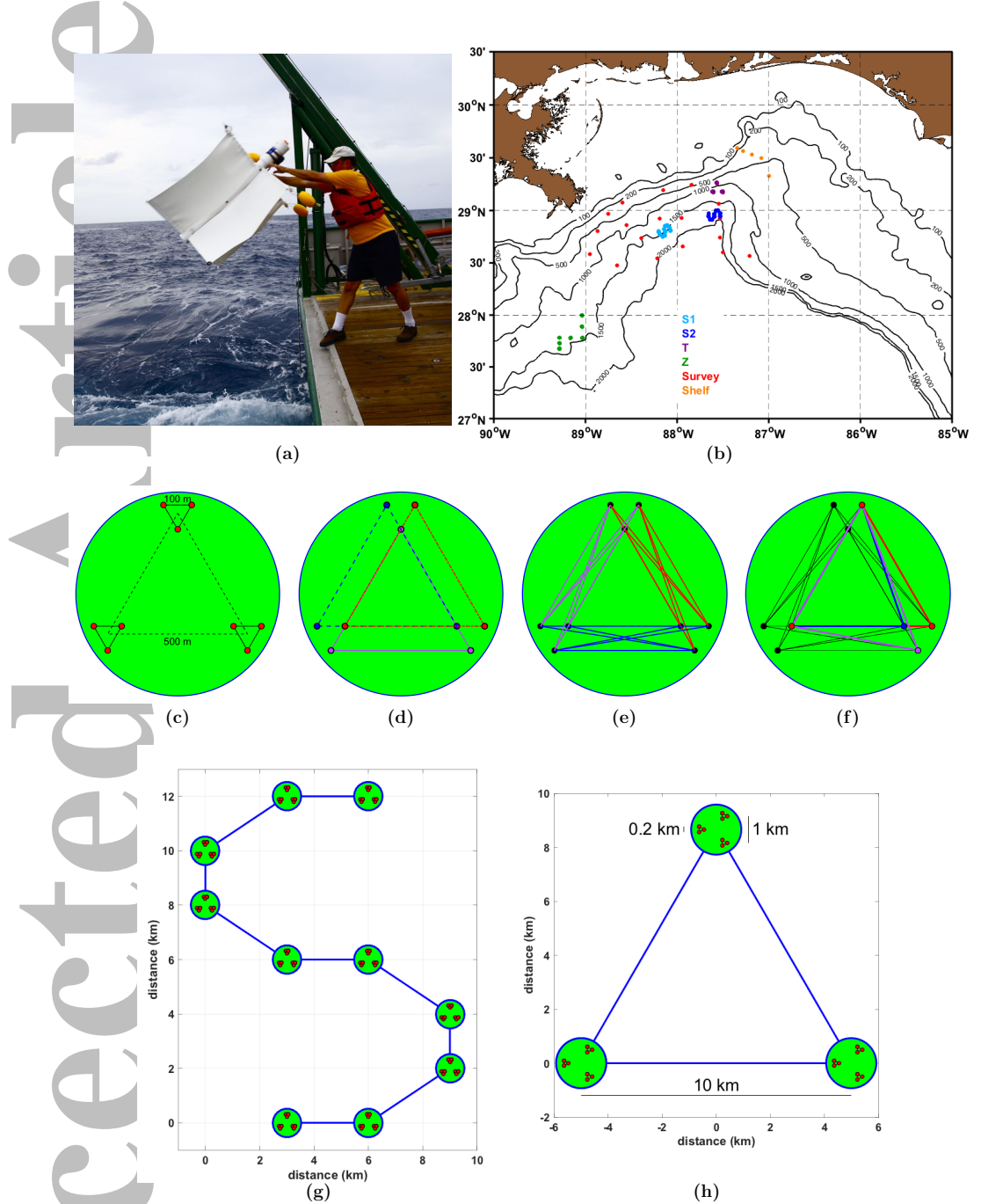


Figure 1. (a) A GLAD drifter being deployed off the *R/V Walton Smith*. (Photo courtesy of T. Özgökmen.) (b) Launch locations for all 295 GLAD drifters. (c) A node of 9 drifters in nested triangles. (d) The 3 independent triangles in a node. (e) The 3 color-coded groups of 9 pairs each at the 500-m scale in a node. Note that within each group 4 pairs are difficult to distinguish, since the 4 distinct endpoints align. (f) The 27 triangles at the 500-m scale in a node, with repeat use of drifters. Three of the triangles that have two drifters in common are highlighted for illustration. (g) ‘S’-shaped deployment pattern. (h) Triply nested triangle deployment pattern.

One of the main objectives of the field campaign was to measure scale-dependent dispersion statistics. For this reason, nested triangles were chosen as the fundamental deployment unit (Fig. 1c), which guaranteed repeat samples at multiple scales. At the smallest scale, the target pattern called for equilateral triangles with side-length 100 m. These were arranged in an equilateral triangle configuration with side-length 500 m. Such a set of nine drifters composed a deployment node, and multiple nodes were combined into larger deployment patterns.

Fig. 1b shows the launch locations of all 295 drifters. Two sets of ninety drifters each were launched in ‘S’-shaped configurations (Fig. 1g) consisting of ten nodes of nested triangles each (hereafter referred to as the *S1* and *S2* launches). A step-shaped configuration was chosen for sampling a cyclone and consisted of seven standard nodes total (hereafter referred to as the *Z* launch). Finally, 27 drifters were arranged in triply nested triangles (Fig. 1h) at launch: three nodes with doubled length scales (200 m and 1000 m) arranged in an equilateral triangle of side-length 10 km (hereafter referred to as the *T* launch). In addition, twenty drifters were released individually as part of a large-scale survey of the region around the DeSoto Canyon before the main part of the experiment, and five more individual drifters were deployed later on the shelf. These individual drifters will not be considered here.

Here we will focus on the data from the first 30 days after deployment; see Fig. 2. More precisely, each triplet will be followed for 30 days following the release of the last of its member drifters. About 8.5% of the trajectories (23) stopped before the end of two weeks, while more than 76.5% (206) persist for the entire 30-day period. Some samples dropping out over time can affect the time series of the statistics. This will be taken into account in the analysis.

2.2 Metrics

Several metrics are introduced to quantify anisotropy and inhomogeneity. Since a standard metric for particle dispersion is pair separation, we focus on statistics based on this quantity for both purposes. These are supplemented with triplet-based statistics.

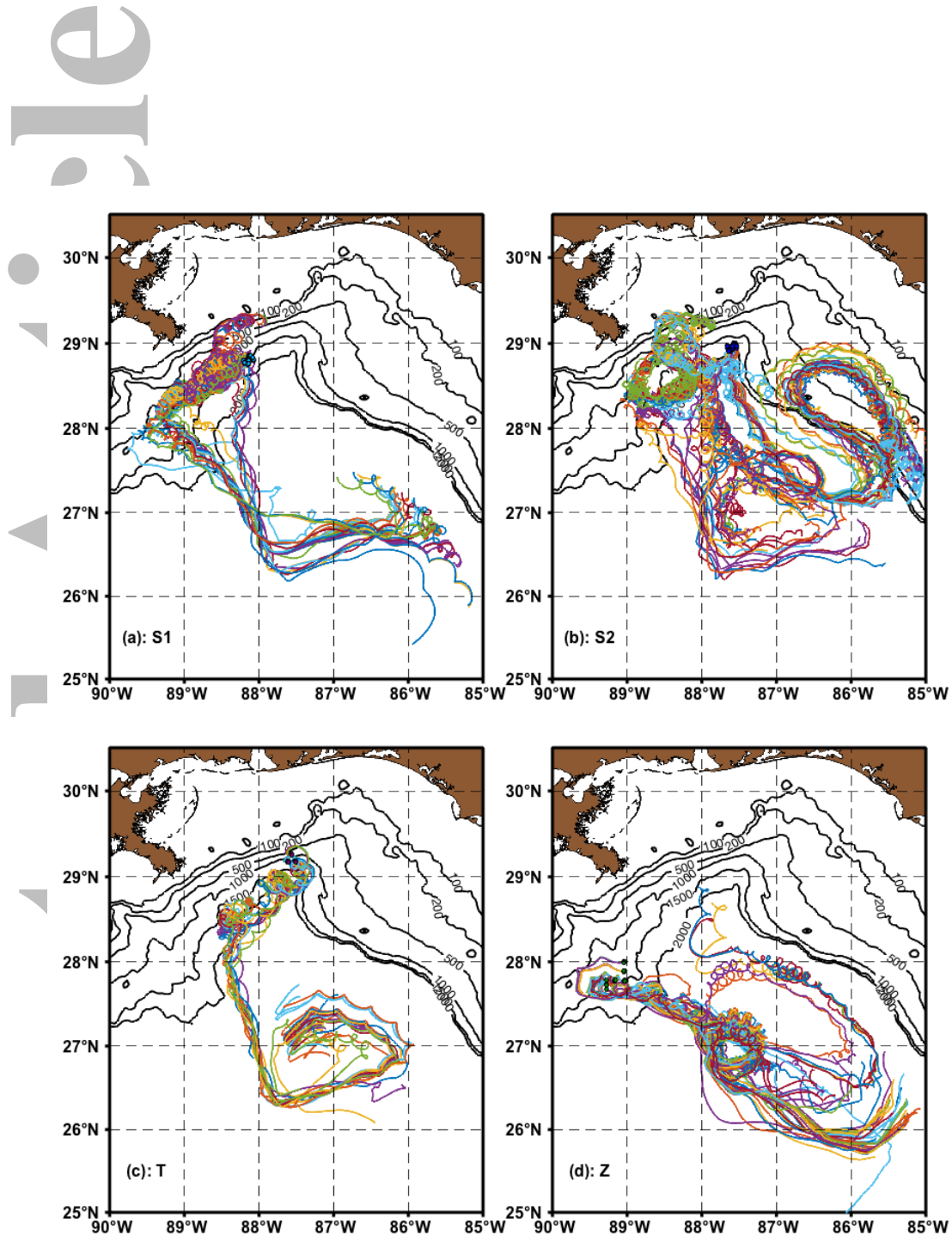


Figure 2. Thirty-day trajectories for each of the deployments: (a) *S1*; (b) *S2*; (c) *T*; and (d) *Z*. A variety of colors is used for illustrative purposes only.

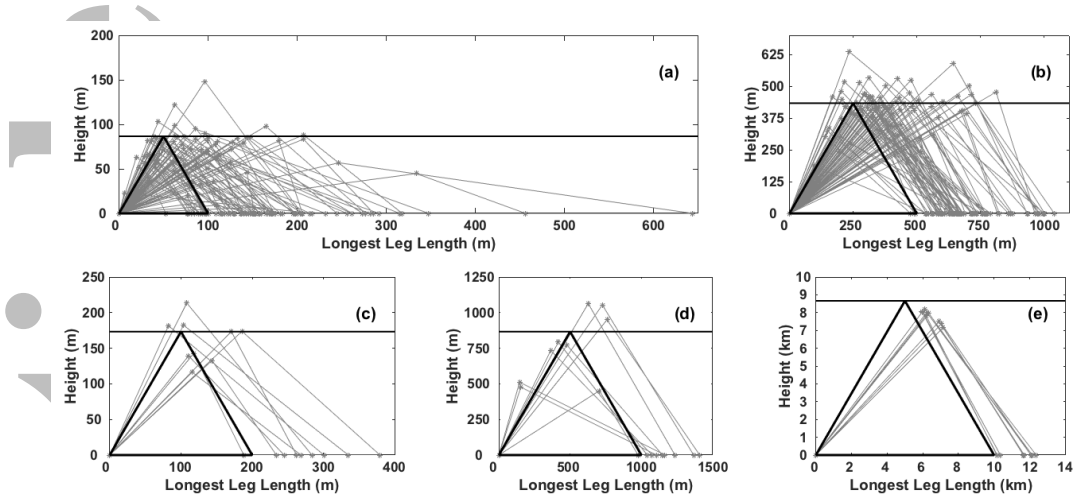


Figure 3. Triangle shapes at the first common data point, mapped to align the longest leg with the x -axis with one corner at the origin. The thick black outline shows the targeted shape, while the grey lines give the realized shapes. (a) 100 m triangles and (b) 500 m triangles from $S1$, $S2$, and Z . (c) 200 m triangles, (d) 1 km triangles, and (e) 10 km triangles from T . Axes on all plots are scaled differently to accommodate the different scales.

165 2.2.1 Anisotropy metric

166 A triangular launch configuration provides three drifter pairs that are nearly colo-
 167 cated. However, each pair samples a different direction. For perfectly locally isotropic
 168 flows, all three pairs should separate at the same rate. Thus, variability across the three
 169 samples is a sign of anisotropy. For easier comparison across scales, the standard devi-
 170 ation is normalized by the mean pair separation across the triplet at a given point in time.
 171 We denote this metric by V_{iso} . The greater V_{iso} , the greater is the anisotropy in the sam-
 172 pled pairs.

173 Of the 270 drifters launched in triplets, all but one reported useful data for at least
 174 5 days. Therefore, there are 80 independent triads at the 100-m scale (three per node
 175 in $S1$, $S2$, and Z , with one missing) and nine at the 200-m scale (three per node in T).
 176 The deployment scheme also permits the construction of triangles with nominal side lengths
 177 of 500 m (scale of a node for $S1$, $S2$, and Z), 1 km (scale of a node for T), and 10 km
 178 (scale of T). An illustration at the nodal scales is given in Fig. 1d. There are 80 inde-
 179 pendent triads at the 500-m scale (again three per node in $S1$, $S2$, and Z , with one miss-
 180 ing), and nine each at the 1-km and 10-km scales.

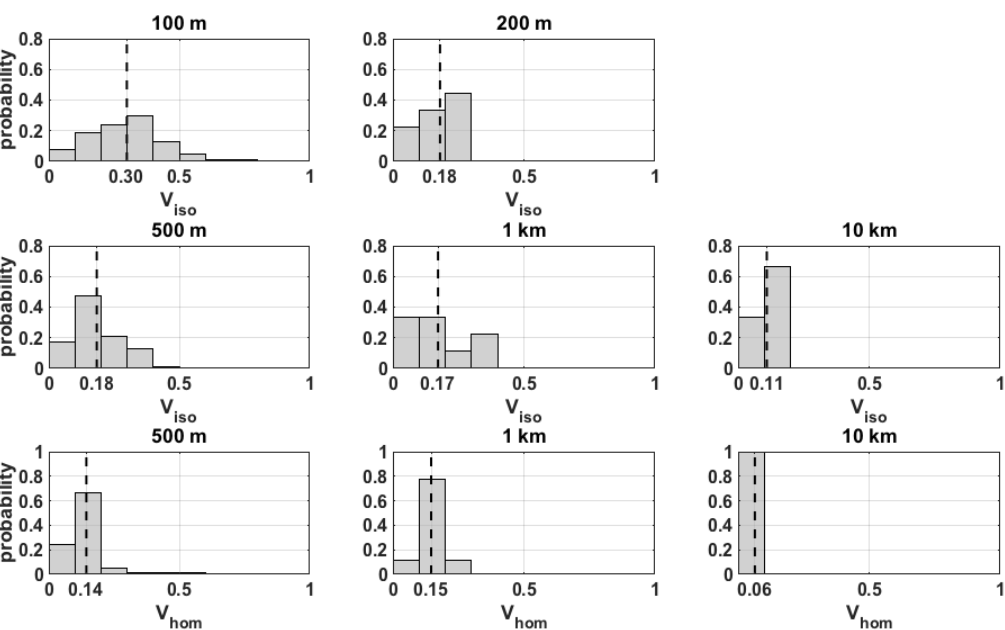


Figure 4. Top and middle rows: Variability of initial pair separations within individual triangles as measured by V_{iso} . Bottom row: Variability of initial pair separations across groups of nearly colocated drifter pairs as measured by V_{hom} . Histograms are shown for the available scales, and the vertical axis is normalized as a probability. The mean value is indicated with a dashed line. Note that there are only three samples for V_{hom} at the 10-km scale.

181 Note that $V_{iso} \neq 0$ even at launch, since the drifters are realistically not released
 182 in perfectly equilateral triangles. Fig. 3 shows the shapes for the initial triangles at each
 183 of the scales. Clearly, some triads are more deformed than others, and V_{iso} at launch varies.
 184 The histograms of V_{iso} at launch for the different scales are given in Fig. 4, top and mid-
 185 dle row. Initial pair separation variability is, on average, greatest at the smallest scale
 186 (0.30) and least at the largest scale (0.11). Except at the 100-m scale, initial V_{iso} val-
 187 ues fall below 0.5.

188 2.2.2 Inhomogeneity metric

189 The deployment configuration does not permit the assessment of inhomogeneity
 190 at the base scales of 100 m and 200 m. Within a standard node, there are 27 pairs with
 191 an initial separation of nominally 500 m. To avoid conflating anisotropy effects with in-
 192 homogeneity effects, these are separated into three groups of pairs, according to the triplets
 193 from which the members are drawn. See Fig. 1e. Within each of these groups, the pairs
 194 are more or less aligned in the same direction, and they have endpoints within 100 m
 195 of each other. Over the 26 complete nodes in $S1$, $S2$, and Z , there are, therefore, 79 such
 196 groups with nine members each; the node with the missing drifter generates three groups
 197 as well, but two of them only have six members each. Similar groups can be formed for
 198 the larger nodes of the T launch, resulting in nine groups with nine pairs each at the 1-
 199 km scale, and for the T launch as a whole, resulting in three groups with 81 pairs each
 200 at the 10-km scale.

201 Variability across the samples within a group is an indication of the influence of
 202 small variations in the initial positions and thus of the inhomogeneity. We proceed as
 203 before and scale the standard deviation in the pair separation by the mean across each
 204 group, denoting the resulting metric as V_{hom} . Because of imperfect launches, V_{hom} , too,
 205 is not exactly 0 at the start. Fig. 4, bottom row, displays the histograms of V_{hom} at launch
 206 for the three sampled scales. For the largest scale, all three samples have $V_{hom}(0) < 0.1$.
 207 This is a result of the deviations from an ideal launch pattern due to practicalities in the
 208 field being small relative to the target scale of 10 km. For the other scales, the variabil-
 209 ity across nearly colocated pairs is on average about 0.15, although there are three out-
 210 liers (out of 81 samples) with values above 0.3 for the 500-m scale.

211 **2.2.3 Triplet metrics**

212 Pair separation has been a popular relative dispersion metric in part because it can
 213 be computed from just two drifters. Since drifter observations have historically been sparse,
 214 this is a great advantage. However, the triplet configurations of the GLAD dataset can
 215 be exploited to investigate additional metrics.

216 Thus, relative dispersion can be computed over a group of three, instead of two,
 217 drifters. One intuitive way to do this is to use the radius of gyration R , defined by $R^2 =$
 218 $\sum_{i=1}^3 r_i^2$, where r_i is the distance of the i th drifter from the center of mass of the triplet.
 219 It turns out that R is equivalent to the RMS of the triangle's side lengths (LaCasce, 2008).
 220 Therefore, the RMS radius of gyration – taken over a collection of triangles – is iden-
 221 tical to the RMS pair separation for pairs within triangles. An alternative metric for the
 222 expansion of the group is the area covered by the triangle, which is not directly related
 223 to the RMS pair separation. It should be noted that three points make a sparse defini-
 224 tion of the perimeter of the water mass initially enclosed by the triangle, so that the time
 225 series of triangle area is better thought of as a metric of the 2D separation of the three
 226 vertices than as a metric of growth of the triangle itself, especially over long time peri-
 227 ods.

228 The driver of local anisotropy is shear. Without shear, a triangle might rotate and
 229 grow or shrink, but it would not change its shape. Thus, shape deformation can be used
 230 as an isotropy metric. A variety of different metrics have been suggested in the litera-
 231 ture (Pumir et al., 2000; Cressman et al., 2004; Merrifield et al., 2010). Here we consider
 232 two. The first is the elongation metric

$$\Lambda = 12\sqrt{3} \frac{A}{P^2}, \quad (1)$$

233 where A denotes the area of the triangle defined by three drifters and P is its perime-
 234 ter (e.g., Berta et al., 2016). The coefficient is chosen so that $\Lambda \in [0, 1]$, with $\Lambda = 0$
 235 for collinear points and $\Lambda = 1$ for equilateral triangles.

236 The second is a function of the ellipticity ($\epsilon = 1 - b/a$) of the minimum-area el-
 237 lipse enclosing the three drifters:

$$E = 1 - \epsilon = \frac{b}{a}, \quad (2)$$

238 where a and b are the lengths of the major and minor axes, respectively. E also varies
 239 between 0 and 1, with $E = 0$ if the drifters have collapsed to a line and $E = 1$ if the

240 three drifters are equally spaced from each other, as in an equilateral triangle. This met-
 241 ric is the reciprocal of the variance aspect ratio in principal axis coordinates used by Ohlmann
 242 et al. (2019).

243 Each node gives rise to 3 triplets at the base scale of 100 m (200 m for the T launch),
 244 as shown in Fig. 1c, plus 27 nearly colocated triads with side-lengths 500 m (1 km for
 245 T), as illustrated in Fig. 1f. For purposes of measuring inhomogeneity, the triads at the
 246 500-m and 1-km scales were grouped by node. This results in 26 groups of 27 triads each
 247 and one group with 18 triads (because of the one missing drifter) at the 500-m scale, and
 248 three groups with 27 triads each at the 1-km scale. At 10 km, triplets were grouped so
 249 that vertices are offset about 200 m (i.e., all members in a group draw from the same
 250 three fundamental triplets), yielding 27 groups with 27 members each. Inhomogeneity
 251 can then be assessed across the area metric, similar to the procedure applied to pair sep-
 252 arations: The standard deviation of the area within a group is scaled by the mean. The
 253 resulting metric is denoted as V_{area} . At launch, $V_{area} = 0.21$ on average at 500 m and
 254 1 km and 0.02 at 10 km.

255 3 One-Dimensional Dispersion: Pair Separation

256 The classic metric for one-dimensional dispersion is pair separation (LaCasce, 2008,
 257 and references therein). Typically, relative dispersion is calculated as the RMS of pair
 258 separation time series over a large group with initially similar separation. These means
 259 are representative under assumptions of homogeneity, isotropy, and stationarity. The fol-
 260 lowing subsections will explore the validity of the first two of these assumptions.

261 Fig. 5 shows the time series of RMS pair separations at each of the scales targeted
 262 with the deployment scheme (100 m, 200 m, 500 m, 1 km, and 10 km), computed sep-
 263 arately for each of the four deployments. Similar results were reported by Poje et al. (2014)
 264 for $S1$ and $S2$ at initial separation scales of 100 m, 500 m, 5 km, and 10 km. Our cal-
 265 culations differ slightly from those by Poje et al. (2014), since our groups were constructed
 266 from initial target separations instead of actual achieved separations. In addition, for con-
 267 sistency in the time series, we include only pairs with reported positions for the entire
 268 30-day period. However, these details do not affect the qualitative results.

269 Drifter pairs across all initial separations experience an RMS separation of $O(100)$ km
 270 after 30 days. This appears to be a characteristic scale of the dynamics in this part of

AACE
tice

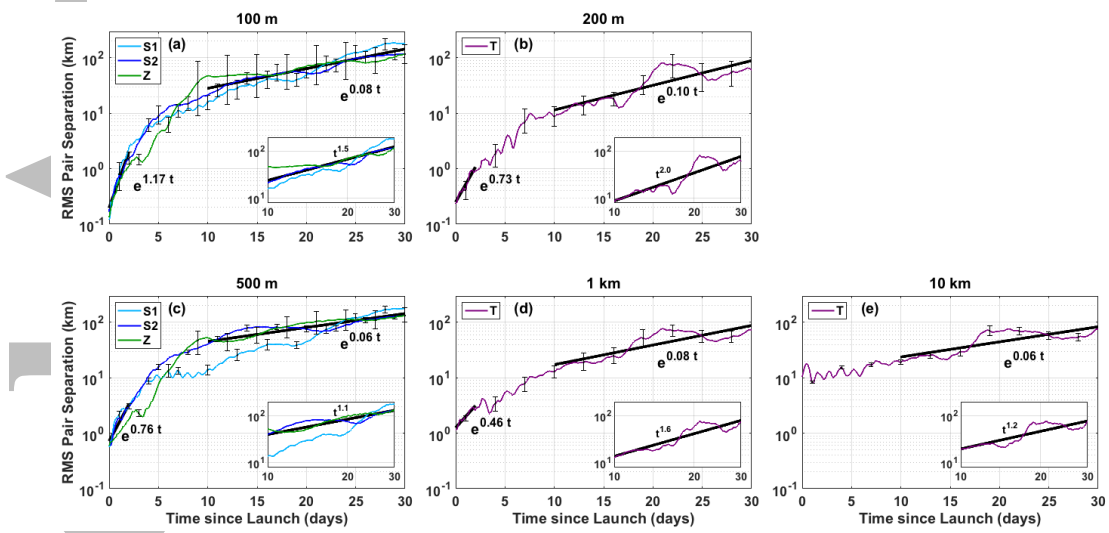


Figure 5. Time series of the RMS pair separations at the different scales. (a) 100 m; (b) 200 m; (c) 500 m; (d) 1 km; (e) 10 km. Colors indicate different deployments: $S1$ in light blue, $S2$ in dark blue, Z in green, and T in purple. Error bars indicate the 95% confidence interval, computed from 2000 bootstrap samples. The exponential growth rates of least squares fits to the combined data from all deployments from the first 2 days (except in (e)) and from the last 20 days are shown. The insets in each panel zoom in on the last 20 days in a log-log plot to illustrate power-law fits over this time interval.

the Gulf of Mexico and is consistent with the notion that the long-term fate of the drifters is driven by the mesoscale. Pairs beginning at small separations initially experience fast dispersion, which is approximately exponential with growth rate around 1.2 at the 100-m scale, 0.75 at the 200-m and 500-m scales, and 0.5 at the 1-km scale for the first 2 days. RMS separations of $O(10)$ km are reached after about a week. The dispersion then slows in subsequent days as separations approach 100 km, with exponential growth rates around 0.06 – 0.10 for the last 20 days. Alternatively, power laws can be fitted to the later time interval, giving exponents of roughly 1 at the 500-m and 10-km scales, of roughly 1.5 at the 100-m and 1-km scales, and of roughly 2.0 at the 200-m scale.

The goodness of fit of these models can be assessed using the index of agreement (Legates & McCabe Jr., 1999)

$$c = 1 - \frac{\sum (m_i - y_i)^2}{\sum (|m_i - \langle y_i \rangle| + |y_i - \langle y_i \rangle|)^2} \quad (3)$$

where y_i is the data, m_i the model prediction, and $\langle \cdot \rangle$ indicates the mean over i . The index takes values between 0 and 1, with higher values associated with better fits. All the exponential fits for the early time interval have c of 0.97 to 0.99, indicating excellent agreement of the model to the data. At the 100-m and 500-m scales, where more data is available, both the exponential and power law fits over the later time interval also have high c values of 0.98 or higher; the exponential fits slightly outperform the power-law fits, by about 0.01, but we do not consider this to be significant. Fits for the later time interval to data from the T launch have c of 0.80 to 0.87, with the power laws slightly outperforming the exponential fits (by about 0.03), although, again, this is not conclusive evidence to prefer one over the other.

Several previous studies of the evolution of drifter pair separations, in various regions of the world's oceans, have found exponential growth in early stages, followed by power-law type growth later (e.g., LaCasce & Ohlmann, 2003; Koszalka et al., 2009; Lumpkin & Elipot, 2010; Schroeder et al., 2011; Zavala Sansón et al., 2017). Reported e-folding rates range from 0.25 (Zavala Sansón et al., 2017) to 1.19 (Koszalka et al., 2009). Our values fall into the upper end of this range. Power law exponents have generally been reported as being close to one of the theoretical values of 0.5 for a diffusive regime, 1 for ballistic motion, or 1.5 for Richardson dispersion. At all but the 200-m scale, our values are comparable to those in the literature. The outlier at 200 m of 2.0 might be a result of the small sample size, with only 14 pairs available at this scale. Confusingly, how-

302 ever, there is no conclusive transition with increasing scales between Richardson and bal-
 303 listic regimes, nor are different turbulence theory regimes consistently associated with
 304 different deployments. What remains clear nonetheless is that the initial fast growth pe-
 305 riod seen at scales less than 10 km is followed by a longer period of much slower growth
 306 in pair separations.

307 The time series are by no means monotonic. Especially *S1* drifters experience sig-
 308 nificant oscillations in their RMS pair separations. These reflect the near-inertial oscil-
 309 lations dominating almost all *S1* trajectories, as seen in Fig. 2(a) and reported by Mariano
 310 et al. (2016). At the 100-m scale, the three deployments show consistent statistics, ex-
 311 cept that *Z* pairs linger for an extra 1.5 days at the $O(1)$ -km separation. At the 500-m
 312 scale, greater geographic variability is visible, with *Z* drifters again dispersing more slowly
 313 up to $O(20)$ km and *S1* drifters taking a week longer to disperse from $O(10)$ km. How-
 314 ever, after about 3 weeks, all pairs show statistically consistent RMS separations near
 315 70 to 100 km, as indicated by the 95% confidence intervals, derived from 2000 bootstrap
 316 samples.

317 3.1 Anisotropy in Pair Separations

318 To investigate anisotropy among drifter pairs, the three pairs within each launch
 319 triangle are compared (Section 2.2.1). A variety of different patterns is observed in these
 320 groups of three time series: When two drifters in a triangle stay close together, the re-
 321 sult is two pair separation time series that track each other, while the third pair remains
 322 at relatively small distances (cf. Fig. 6(a)). Sometimes, first one drifter separates from
 323 the other two, then rejoins the group, before a different drifter separates from the remain-
 324 ing two (cf. Fig. 6(b)). Often, the three pair separation time series track each other more
 325 closely (cf. Fig. 6(c)), which reflects greater isotropy. For some examples, the character
 326 of the anisotropy is variable over time (cf. Fig. 6(d)).

327 The degree of isotropy is quantified using the metric V_{iso} (Section 2.2.1), the stan-
 328 dard deviation across each triplet normalized by the mean pair separation. Each of the
 329 examples on the left in Fig. 6 is accompanied by its time series of V_{iso} . These show sig-
 330 nificant variability in time. However, the qualitative impression of greater anisotropy for
 331 the example in panel (a) is confirmed by higher values for V_{iso} (around 0.75 on average
 332 versus 0.36 – 0.66 for the other examples).

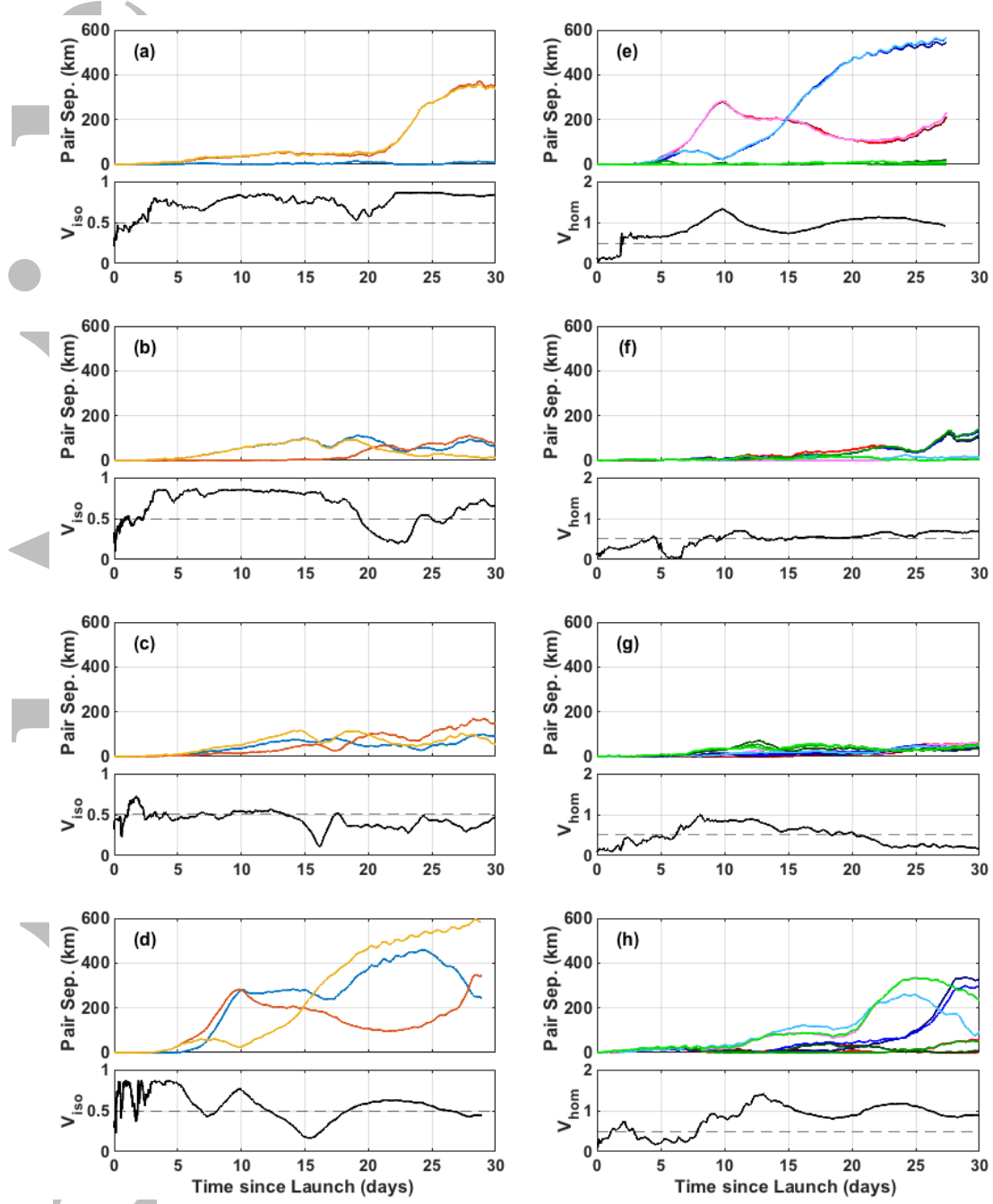


Figure 6. (Left) Time series of pair separations and associated V_{iso} for four example groups of three pairs each, launched at an initial nominal separation distance of 100 m with different orientation. (Right) Time series of pair separations and associated V_{hom} for four example groups of six nearly co-located pairs oriented in the same direction, launched at an initial nominal separation distance of 500 m. Different colors indicate different pairs. For the right panels, blues share one endpoint, as do reds and greens; dark shades also share one endpoint, as do medium and light shades. (a) Two time series separate from the third. (b) Two pairs exhibit similar separation evolution, but the pair identities switch. (c) and (d) Two representative examples of other observed patterns. (e) and (f) Pair separations are sensitive to one endpoint only. (g) Predominantly homogeneous dispersion. (h) Predominantly inhomogeneous dispersion.

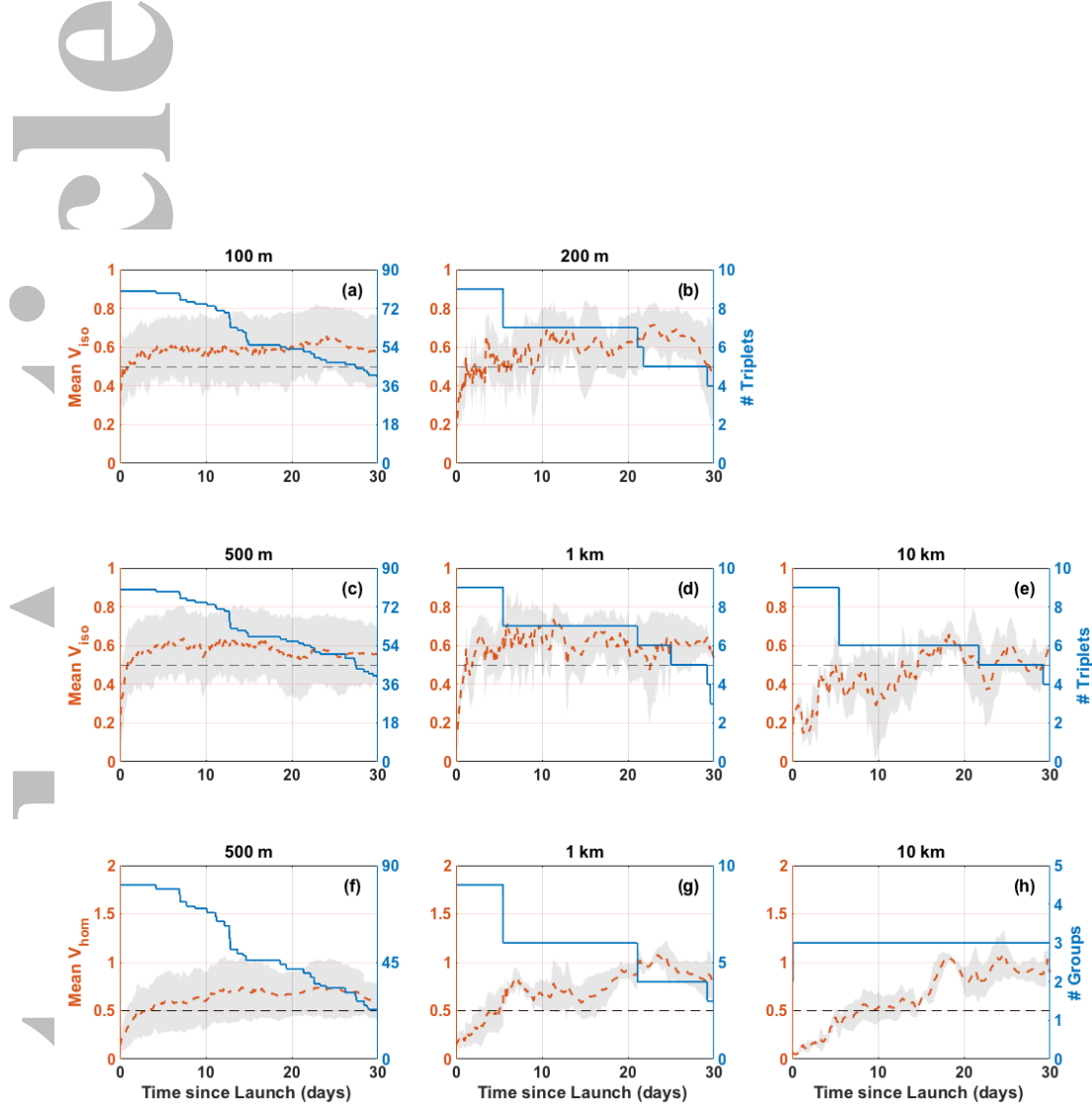


Figure 7. Red: (Top and middle rows) Time series of the mean V_{iso} (red) with one-standard-deviation envelope (grey shading) for (a) 100-m, (b) 200-m, (c) 500-m, (d) 1-km, and (e) 10-km initial separation triplets. (Bottom) Time series of mean V_{hom} (red) with one-standard-deviation envelope (grey shading) for (f) 500-m, (g) 1-km, and (h) 10-km initial separation triplets. Blue: Number of groups that entered the calculation. Note that many more samples were available for (a) and (c) than for (b), (d), and (e). For (f) and (g), only complete groups, i.e., those with all 9 pairs reporting, were used. At the 10-km scale, each group consists of 81 pairs. After 30 days, all three groups had 24 to 54 pairs reporting, which was deemed sufficient for the statistics.

333 Fig. 7(a)–(e) shows the time series of ensemble mean V_{iso} for 30-days following launch
 334 for each of the sampled scales. Note that the 100-m and 500-m scales are sampled by
 335 the $S1$, $S2$, and Z deployments for a total of potentially 81 triplets, whereas the other
 336 scales are sampled only in the T launch, which produced only 9 independent triplets at
 337 each scale. Therefore the results for these scales (Fig. 7(b), (d), and (e)) are noisier. Sim-
 338 ilarities can be observed across all scales less than 10 km: There is a sharp increase in
 339 V_{iso} during the first 1-2 days, followed by a leveling off with oscillations around $V_{iso} =$
 340 0.6. At the largest scale of 10 km, V_{iso} increases over a longer time period, then oscil-
 341 lates about 0.5. These results are consistent with the flows at larger scales yielding more
 342 isotropic dispersion, as drifter pairs at these separations no longer sample the energetic
 343 submesoscale flows driving frontogenesis and other anisotropic phenomena.

344 3.2 Inhomogeneity in Pair Separations

345 Inhomogeneity is assessed at the larger scales (500 m, 1 km, and 10 km) by study-
 346 ing the variability over groups of pairs that are nearly aligned but have slightly differ-
 347 ent endpoints. For the 500-m, 1-km, and 10-km scales, the endpoints are within 100 m,
 348 200 m, and 1 km, respectively. The right column of Fig. 6 displays four examples of vari-
 349 ability in the pair separations across these groups, along with the associated V_{hom} . A
 350 variety of different patterns occurs in the V_{hom} time series: Initial values may stay low
 351 for 1-2 days (examples (e) and (f)) or increase immediately (example (h)). V_{hom} may
 352 stay relatively constant for 15-20 days (examples (e) and (f)) or increase and decrease
 353 alternately (example (g)). The average behavior for each scale is shown in Fig. 7(f)–(h).
 354 After 3 to 7 days the mean V_{hom} exceeds 0.5 and remains there. Unlike for V_{iso} , there
 355 is no clear saturation within the 30 days for the 1-km and 10-km scales, and V_{hom} con-
 356 tinues to increase, though not monotonically, over time. For the 500-m scale, it settles
 357 around 0.7. Greater inhomogeneity at larger scales is not unexpected, since the initial
 358 separation between different pairs is also larger, providing more opportunity to be sub-
 359 jected to different localized flows.

360 4 Two-Dimensional Dispersion

361 The nested triangle launch configuration used in GLAD generates many drifter pairs
 362 that can be grouped to investigate anisotropy and inhomogeneity, as seen in the previ-
 363 ous section. It is also ideal for studying drifter triplets. Three is the minimum number

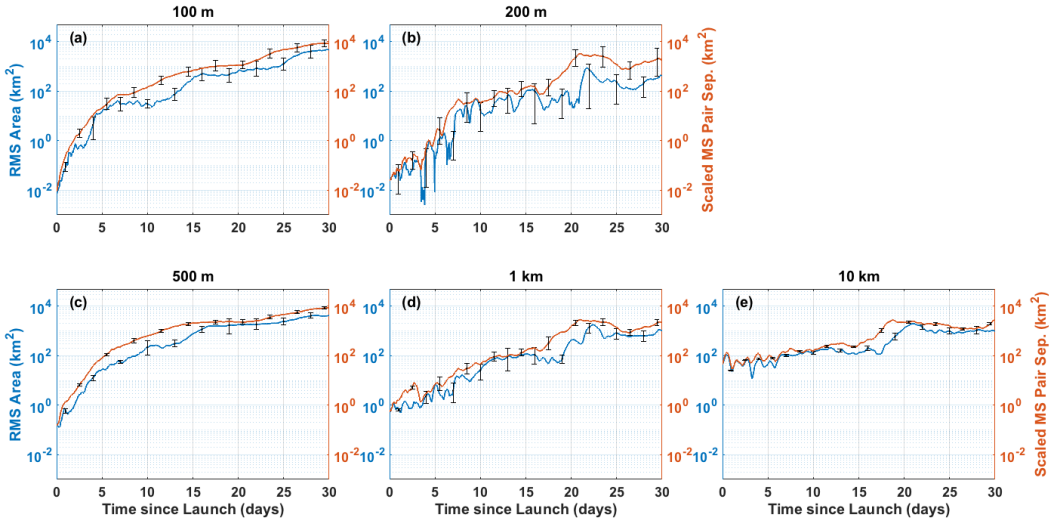


Figure 8. Time series of the (blue) RMS area and (red) mean-square pair separation scaled by $\sqrt{3}/4$ at the different scales. (a) 100 m; (b) 200 m; (c) 500 m; (d) 1 km; (e) 10 km. Error bars indicate the 95% confidence interval, computed from 2000 bootstrap samples.

of drifters for sampling both spatial dimensions simultaneously. When computing the radius of gyration as a dispersion metric, however, this additional information is lost. (See the discussion in Section 2.2.3.) Thus, instead, we will consider triangle area.

4.1 Area Expansion

Quite a few drifters from *S1* were lost after about 12.5 days; by 30 days, only 8 of 81 triplets at the 100-m scale are still complete. Thus, statistics for separate deployments over the 30-day period were not computed. Fig. 8 shows the time series of RMS area at each scale, averaged over triplets that stayed complete for 30 days from all deployments. The results are based on 40 samples at the 100-m scale, only 4 samples at the 200-m scale, 345 samples at the 500-m scale, 35 samples at the 1-km scale, and 216 samples at the 10-km scale. Also plotted on the same axes are the mean-square (MS) pair separations computed from the same subsets of the data (i.e., only pairs that are part of surviving triplets), for a direct comparison between the two quantities. For equilateral triangles, the ratio of the two is exactly $\sqrt{3}/4$, and MS pair separation has been scaled by this ratio in the plots. At all scales, the 1D and 2D dispersion estimates exhibit similar growth patterns, although the two curves separately somewhat and RMS area tends to be noisier.

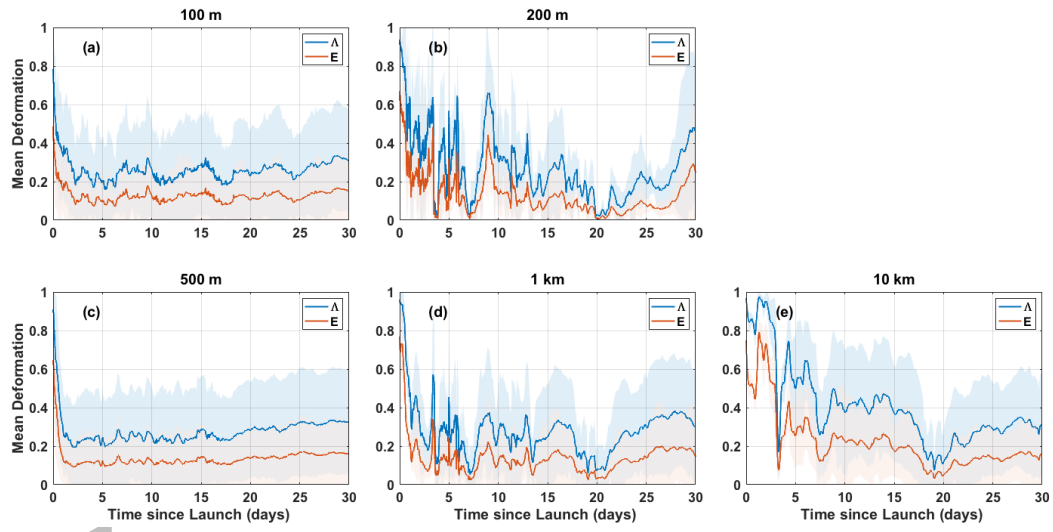


Figure 9. Time series of the mean (blue) Λ and (red) E deformation metrics for (a) 100-m, (b) 200-m, (c) 500-m, (d) 1-km, and (e) 10-km initial separation triplets. Note that for the 200-m scale, only 4 samples were available. Shading shows a one-standard-deviation envelope.

4.2 Anisotropy from Triplets

The anisotropy effects are quantified with the 2D elongation metric Λ and the transformed minimum area ellipticity $E = 1 - \epsilon$, defined in equations (1) and (2) (Section 2.2.3). As triangles deform, under anisotropic dispersion, Λ and E decrease below 1. Fig. 9 illustrates that the two metrics track each other well, although Λ tends to be larger than E . The data from the T launch is characterized by a great deal of variability. Generally, however, at all scales less than 10 km, the deformation metrics on average experience a sharp drop in the first 1 – 2 days, followed by oscillations around relatively low values. More specifically, at the 100-m scale, the mean Λ drops from an initial value of 0.78 to a mean over days 2 – 30 of 0.25 ± 0.04 ; 200 m, it drops from 0.91 to 0.25 ± 0.14 ; at 500 m from 0.89 to 0.27 ± 0.04 ; and at 1 km from 0.96 to 0.26 ± 0.09 . Similarly, at the 100-m scale, the mean E drops from an initial 0.49 to a mean over days 2 – 30 of 0.12 ± 0.02 ; at 200 m from 0.62 to 0.11 ± 0.08 ; at 500 m from 0.62 to 0.13 ± 0.02 ; and at 1 km from 0.77 to 0.12 ± 0.05 . This is qualitatively consistent with the results by Ohlmann et al. (2019), who found a drop of E values from 0.7 – 0.9 to around 0.1 – 0.5 over 4 hours for releases at the 100-m scale. Larger excursions are seen at the 200-m and 1-km scales than at the 100-m and 500-m scales (with 2 to 4 times the standard deviations), but the means are comparable. On the other hand, at the upper end of the sub-

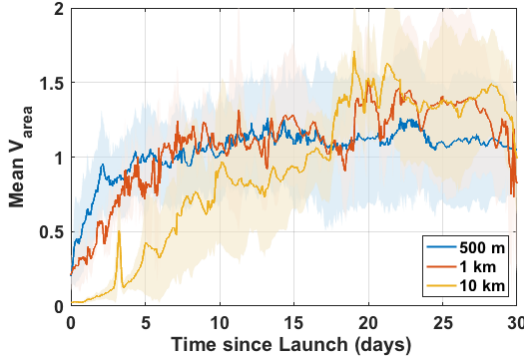


Figure 10. Time series of mean V_{area} for (blue) 500-m, (red) 1-km, and (yellow) 10-km initial separation triplets. Shading shows a one-standard-deviation envelope.

mesoscale, not only does the initial decline last longer — roughly 8 days — the means for the latter part of the time series are also higher, with 0.32 ± 0.10 for Λ and 0.16 ± 0.06 for E . A difference of means test shows significance at the 95% level. Anisotropy effects are reduced for the largest sampled scale, confirming the results from the one-dimensional dispersion analysis in Section 3.1.

It should be noted that the deformation metrics vary greatly over the 30 days for most individual triplets, leading to standard deviations for Λ around 0.25 and for E around 0.15 at each scale (except for the 200-m scale, where they are 0.2 and 0.1, respectively). It is not uncommon for a triplet that has become nearly aligned, with low Λ and E values, to spread again for higher Λ and E at some later point during the 30 days, and vice versa. This indicates that anisotropy affects the triangles throughout the time interval, although most strongly (on average) at the beginning, and that drifter triplets do not tend to reflect isotropic dispersion even after long time periods and at the largest scale, in contrast to the findings of LaCasce and Ohlmann (2003).

4.3 Inhomogeneity from Triplets

The story is more complicated for inhomogeneity effects. Fig. 10 shows the evolution of V_{area} , a measure of the variability in the area defined by a triplet over each group of nearby triplets. At the 500-m scale, on average, V_{area} increases rapidly from an initial value of 0.2 to values around 1 within about 5 days. At 1 km, the behavior is similar, with a slightly less steep initial rise, although the sample size is very small (3 groups).

419 At the largest sampled scale, V_{area} increases more slowly, reaching a value of 1 only af-
 420 ter about 16 days and continuing to rise for another 2 days to level off at a value around
 421 1.4. (The mean values attained over the last 12 analysis days for the 500-m and 1-km
 422 scales, for comparison, are 1.1 and 1.3, respectively.) Again, at the largest scale, the in-
 423 homogeneity effect acts more slowly, but after 30 days the cumulative impact is compa-
 424 rable to that at 1 km.

425 5 Conclusions

426 The wealth of drifter trajectories generated by the GLAD experiment provides a
 427 unique opportunity to assess local isotropy and homogeneity in the dispersion proper-
 428 ties of the flow in the DeSoto Canyon region of the northern Gulf of Mexico. The nested
 429 triplet configuration of the deployment nodes, coupled with the large number of drifters
 430 released, allows for the first time such a statistical analysis across several scales, from
 431 100 m to 10 km.

432 The different anisotropy metrics — V_{iso} , Λ , and E — paint a consistent picture of
 433 local anisotropy affecting drifter samples in the first few days, with little further impacts
 434 at later times. This holds across all scales, although some differences are observed at the
 435 largest scale of 10 km: The initial period of increasing variability lasts longer, namely
 436 1–2 weeks and the anisotropy signature is generally weaker, as more highly anisotropic
 437 flows at smaller scales are no longer resolved. Based on the analysis of V_{iso} , the spread
 438 (as measured by standard deviation) exceeds half of the mean pair separation at times
 439 past the initial adjustment period. This suggests that pair orientation is relevant when
 440 observing the evolution of pair separation at a particular location, as also illustrated by
 441 some of the examples on the left in Fig. 6.

442 In spite of this local anisotropy, one might expect that it averages out regionally.
 443 This is generally the case, at least averaged over multiple deployments. For Fig. 11, nearly
 444 colocated drifter pairs were separated into three groups, to include only one orientation
 445 each. RMS pair separations were then computed and plotted for each set separately. At
 446 100 m (panel (a)) and 500 m (panel (c)), when all three deployments are used, the three
 447 directional estimates agree within the 95% confidence intervals. Fig. 11 (f) – (h) also shows
 448 the results at 500 m for each individual deployment, and agreement varies. In particu-
 449 lar, for Z (panel (h)), RMS pair separation is significantly lower for one of the sampling

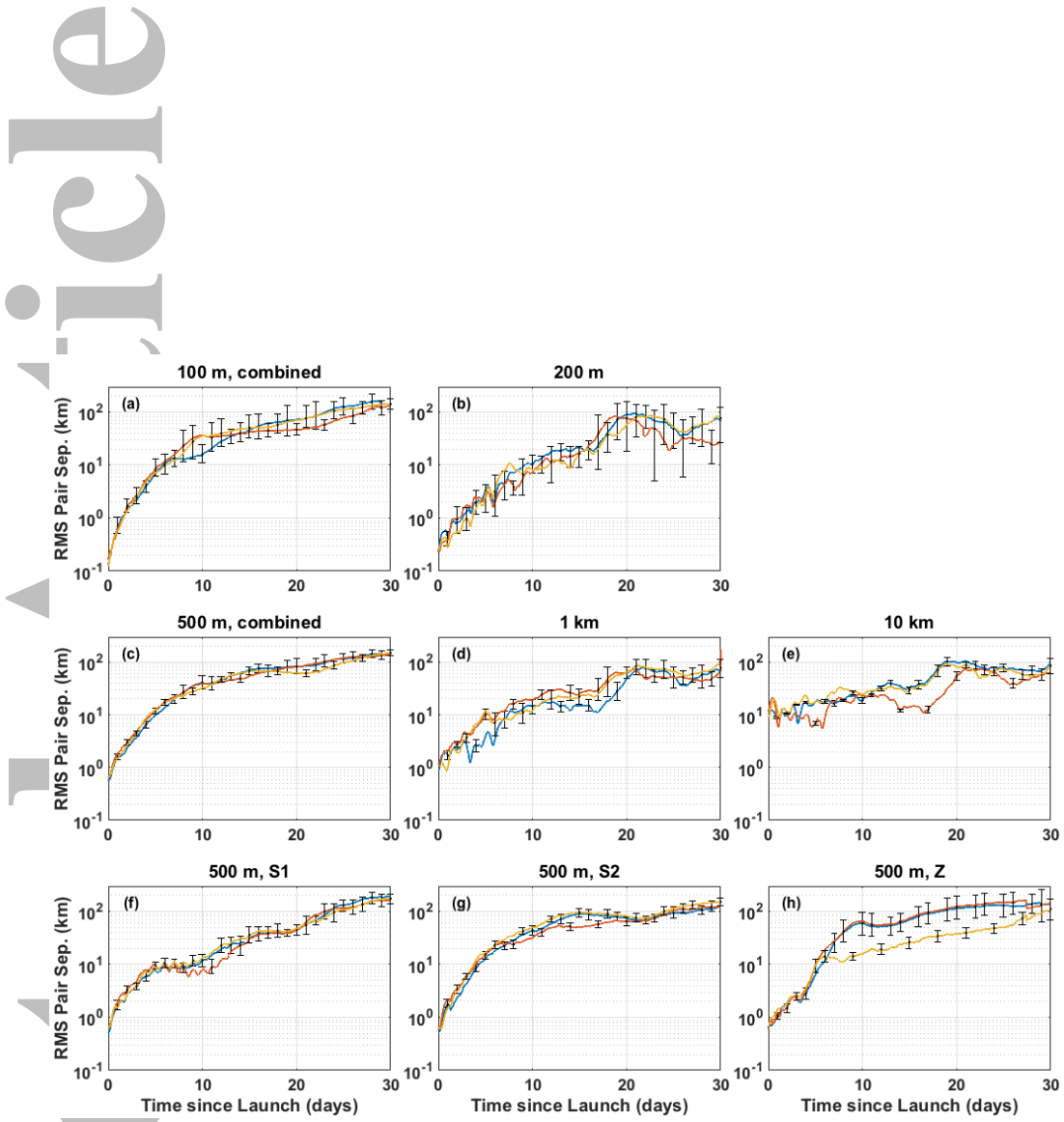


Figure 11. Time series of RMS pair separations computed from three differently oriented subsets of the available pairs, indicated by colors. Each curve uses only nearly aligned pairs, for all available deployments at (a) 100 m, (b) 200 m, (c) 500 m, (d) 1 km, and (e) 10 km and for individual deployments at 500 m, (f) S1, (g) S2, and (h) Z. Error bars indicate the 95% confidence interval, computed from 2000 bootstrap samples.

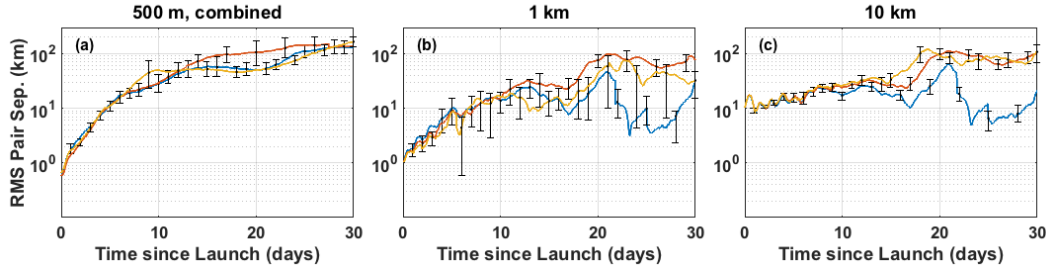


Figure 12. Time series of RMS pair separations computed from three different subsets of the available pairs, indicated by colors, defined by a unique drifter chosen from each of the smallest triplets. (a) 500 m (all deployments), (b) 1 km, and (c) 10 km. Error bars indicate the 95% confidence interval, computed from 2000 bootstrap samples.

directions than for the other two. The same is true for the T launch, at 10 km (panel (e)). The large number of samples results in small error bars, but originating from just one deployment, they sample a limited variety of flows.

By definition, anisotropy is strongest in the principle axes coordinate system, which is captured by the ellipticity metric E . Ohlmann et al. (2019) pointed out that anisotropy computed for geographic coordinates — in their case along- and cross-shore — is comparatively weak, since the responsible processes are not uniformly aligned with these coordinates. The three directions sampled here are not intentionally aligned with any particular forces, and thus the analysis does not identify a particular source. Rather it is intended to reveal the magnitude of the variability in relative dispersion estimates due to local anisotropy. When considering a single deployment, it is more likely that one of the sampled flow directions aligns with the principle axes, resulting in an increased anisotropy signal.

Inhomogeneity was evaluated at scales of 500 m, 1 km, and 10 km, by considering variability over initial displacements of 100 m, 200 m, and 1 km, respectively. Similarly to the anisotropy findings, local inhomogeneity effects are substantial in the first week, as seen in both the pair separation statistic V_{hom} (Fig. 7 (f) – (h)) and the triplet area statistic V_{area} (Fig. 10). For the 500-m scale, they then weaken, whereas at 1 km they weaken for a while, followed by another spurt of growth in variability at the 18-day mark, and at 10 km, the increase in variability persists continuously for the first roughly 20 days.

470 How does local inhomogeneity impact regional averages? We assessed this by tak-
 471 ing three subsets of the dataset, each making use of only one of the three drifters in the
 472 smallest triplets (at 100-m or 200-m spacing, thereby eliminating pairs at these scales).
 473 RMS pair separations are then computed over all pairs within each subset at each scale.
 474 See Fig. 12. The results are similar to those for anisotropy: When averaged over mul-
 475 tiple deployments, as on the 500-m scale (panel (a)), the three estimates generally agree
 476 within their 95% confidence intervals. This is not true at this scale for the *Z* deployment
 477 on its own (not shown), nor at the larger scales that were only sampled in the *T* deploy-
 478 ment (panels (b) and (c)).

479 Thus, the densely deployed GLAD drifters demonstrated that anisotropy and in-
 480 homogeneity in ocean flows, which impact local dispersion statistics, become less impor-
 481 tant when estimates can be made from samples drawn from a large enough region. How
 482 large is large enough depends on the local flow conditions — *S1* and *S2*, e.g., did not show
 483 significant anisotropy effects at 500 m, but *Z* did, even though the latter deployment cov-
 484 ered a larger area. Moreover, the statistics at 10 km exhibited some differences from those
 485 at smaller scales, with longer time scales before anisotropy or inhomogeneity effects sat-
 486 urate. This reflects the transition from submesoscale to mesoscale dynamics.

487 Acknowledgments

488 This work was funded in part by grants N00014-11-1-0087 for MURI *OCEAN 3D+1* and
 489 N00014-18-1-2461 for DRI *CALYPSO* from the Office of Naval Research and in part by
 490 a grant from The Gulf of Mexico Research Initiative for the Consortium for Advanced
 491 Research on Transport of Hydrocarbon in the Environment (CARTHE). The processed
 492 drifter data analyzed here are publicly available through the Gulf of Mexico Research
 493 Initiative Information & Data Cooperative (GRIIDC) at <https://data.gulfresearchinitiative.org>
 494 under doi 10.7266/N7416V0M (Özgökmen, 2013).

495 References

- 496 Bennett, A. F. (1987). A Lagrangian analysis of turbulent diffusion. *Rev. Geophys.*,
 497 25(4), 799–822. doi: 10.1029/RG025i004p00799
- 498 Beron-Vera, F. J., & LaCasce, J. H. (2016). Statistics of simulated and observed pair
 499 separations in the Gulf of Mexico. *J. Phys. Oceanogr.*, 46(7), 2183–2199. doi:
 500 10.1175/JPO-D-15-0127.1

- 501 Berta, M., Griffa, A., Özgökmen, T. M., & Poje, A. C. (2016). Submesoscale evo-
 502 lution of surface drifter triads in the Gulf of Mexico. *Geophys. Res. Lett.*,
 503 43(22), 11,751–11,759. doi: 10.1002/2016GL070357
- 504 Berti, S., Santos, F. A. D., Lacorata, G., & Vulpiani, A. (2011). Lagrangian drifter
 505 dispersion in the southwestern Atlantic Ocean. *J. Phys. Oceanogr.*, 41(9),
 506 1659–1672. doi: 10.1175/2011JPO4541.1
- 507 Capet, X., McWilliams, J. C., Molemaker, M. J., & Shchepetkin, A. F. (2008).
 508 Mesoscale to submesoscale transition in the California Current System. part i:
 509 Flow structure, eddy flux, and observational tests. *J. Phys. Oceanogr.*, 38(1),
 510 29–43. doi: 10.1175/2007JPO3671.1
- 511 Corrado, R., Lacorata, G., Palatella, L., Santoleri, R., & Zambianchi, E. (2017).
 512 General characteristics of relative dispersion in the ocean. *Scientific Reports*,
 513 7, 46291. doi: 10.1038/srep46291
- 514 Cressman, J. R., Goldburg, W. I., & Schumacher, J. (2004). Dispersion of tracer
 515 particles in a compressible flow. *Europhys. Lett.*, 66(2), 219–225. doi: 10.1209/
 516 epl/i2003-10187-x
- 517 D'Asaro, E. A., Shcherbina, A. Y., Klymak, J. M., Molemaker, J., Novelli, G.,
 518 Guigand, C. M., ... Özgökmen, T. M. (2018). Ocean convergence and the
 519 dispersion of flotsam. *Proc. Natl. Acad. Sci. USA*, 115(6), 1162–1167. doi:
 520 10.1073/pnas.1718453115
- 521 Davis, R. E. (1985). Drifter observations of coastal surface currents during CODE:
 522 The method and descriptive view. *J. Geophys. Res.*, 90(C3), 4741–4755. doi:
 523 10.1029/JC090iC03p04741
- 524 Gula, J., Molemaker, M. J., & McWilliams, J. C. (2014). Submesoscale cold fila-
 525 ments in the Gulf Stream. *J. Phys. Oceanogr.*, 44(10), 2617–2643. doi: 10
 526 .1175/JPO-D-14-0029.1
- 527 Haza, A. C., Poje, A. C., Özgökmen, T. M., & Martin, P. J. (2008). Relative disper-
 528 sion from a high-resolution coastal model of the Adriatic Sea. *Ocean Model.*,
 529 22(1-2), 48–65. doi: 10.1016/j.ocemod.2008.01.006
- 530 Huntley, H. S., Lippardt Jr., B. L., Jacobs, G. A., & Kirwan Jr., A. D. (2015).
 531 Clusters, deformation, and dilation: Diagnostics for material accumulation re-
 532 gions. *J. Geophys. Res. Oceans*, 120, 6622–6636. doi: 10.1002/2015JC011036
- 533 Jacobs, G. A., Huntley, H. S., Kirwan Jr., A. D., Lippardt Jr., B. L., Campbell,

- 534 T., Smith, T., ... Bartels, B. P. (2016). Ocean processes underlying surface
 535 clustering. *J. Geophys. Res.*, 121, 180–197. doi: 10.1002/2015JC011140
- 536 Kirwan, A. D., Jr. (1969). Formulation of constitutive equations for large-scale tur-
 537 bulent mixing. *J. Geophys. Res. - Oceans*, 74(28), 6953–6959. doi: 10.1029/
 538 JC074i028p06953
- 539 Kirwan, A. D., Jr., McNally, G. J., Reyna, E., & Merrell, W. J., Jr. (1978). The
 540 near-surface circulation of the eastern North Pacific. *J. Phys. Oceanogr.*, 8(6),
 541 937–945. doi: 10.1175/1520-0485(1978)008<0937:TNSCOT>2.0.CO;2
- 542 Koszalka, I. M., LaCasce, J. H., & Orvik, K. A. (2009, July). Relative dis-
 543 persion in the Nordic Seas. *J Mar Res*, 67(4), 411–433. doi: 10.1357/
 544 002224009790741102
- 545 LaCasce, J. H. (2008). Statistics from Lagrangian observations. *Prog. Oceanogr.*,
 546 77(1), 1–29. doi: 10.1016/j.pocean.2008.02.002
- 547 LaCasce, J. H., & Bower, A. (2000). Relative dispersion in the subsurface North At-
 548 lantic. *J. Mar. Res.*, 58(6), 863–894. doi: 10.1357/002224000763485737
- 549 LaCasce, J. H., & Ohlmann, J. C. (2003). Relative dispersion at the sur-
 550 face of the Gulf of Mexico. *J. Mar. Res.*, 61(3), 285–312. doi: 10.1357/
 551 002224003322201205
- 552 Lacorata, G., Aurell, E., & Vulpiani, A. (2001). Drifter dispersion in the Adri-
 553 atic Sea: Lagrangian data and chaotic model. *Annales Geophysicae*, 19(1),
 554 121–129. doi: 10.5194/angeo-19-121-2001
- 555 Lapeyre, G., & Klein, P. (2006). Impact of the small-scale elongated fila-
 556 ments on the oceanic vertical pump. *J. Mar. Res.*, 64(6), 835–851. doi:
 557 10.1357/002224006779698369
- 558 Legates, D. R., & McCabe Jr., G. J. (1999). Evaluating the use of “goodness-of-
 559 fit” measures in hydrologic and hydroclimatic model validation. *Water Resour.
 560 Res.*, 35(1), 233–241. doi: 10.1029/1998WR900018
- 561 Lumpkin, R., & Eliot, S. (2010). Surface drifter pair spreading in the North
 562 Atlantic. *J. Geophys. Res. - Oceans*, 115(C12), C12017. doi: 10.1029/
 563 2010JC006338
- 564 Mantovanelli, A., Heron, M. L., Heron, S. F., & Steinberg, C. R. (2012, November).
 565 Relative dispersion of surface drifters in a barrier reef region. *J. Geophys. Res.
 566 - Oceans*, 117(C11), C11016. doi: 10.1029/2012JC008106

- 567 Mariano, A. J., Ryan, E. H., Huntley, H. S., Laurindo, L. C., Coelho, E. F., Griffa,
 568 A., ... Wei, M. (2016). Statistical properties of the surface velocity field in the
 569 northern Gulf of Mexico sampled by GLAD drifters. *J. Geophys. Res. Oceans*,
 570 121, 5193–5216. doi: 10.1002/2015JC011569
- 571 McWilliams, J. C. (2016). Submesoscale currents in the ocean. *Proc. R. Soc. A*,
 572 472(2189), 20160117. doi: 10.1098/rspa.2016.0117
- 573 Mensa, J. A., Özgökmen, T. M., Poje, A. C., & Imberger, J. (2015). Material
 574 transport in a convective surface mixed layer under weak wind forcing. *Ocean
 575 Model*, 96, 226–242. doi: 10.1016/j.ocemod.2015.10.006
- 576 Merrifield, S. T., Kelley, D. H., & Ouellette, N. T. (2010). Scale-Dependent Statisti-
 577 cal Geometry in Two-Dimensional Flow. *Phys Rev Lett*, 104(25). doi: 10.1103/
 578 PhysRevLett.104.254501
- 579 Meyerjürgens, J., Badewien, T. H., Garaba, S. P., Wolff, J.-O., & Zielinski, O.
 580 (2019). A state-of-the-art compact surface drifter reveals pathways of float-
 581 ing marine litter in the German Bight. *Front. Mar. Sci.*, 6, 197–15. doi:
 582 10.3389/fmars.2019.00058
- 583 Ohlmann, J. C., Romero, L., Pallàs-Sanz, E., & Perez-Brunius, P. (2019).
 584 Anisotropy in coastal ocean relative dispersion observations. *Geophys. Res.
 585 Lett.*, 32(7), 2171. doi: 10.1029/2018GL081186
- 586 Ollitrault, M., Gabillet, C., & De Verdière, A. C. (2005). Open ocean regimes
 587 of relative dispersion. *J. Fluid Mech.*, 533, 381–407. doi: 10.1017/
 588 S0022112005004556
- 589 Özgökmen, T. M. (2013). *Grand Lagrangian Deployment (GLAD) CODE-style
 590 and flat drifter trajectories (5-min interpolation, no filtering), northern Gulf
 591 of Mexico near DeSoto Canyon, july-october 2012*. Distributed by: Gulf of
 592 Mexico Research Initiative Information and Data Cooperative (GRIIDC),
 593 Harte Research Institute, Texas A&M University – Corpus Christi. doi:
 594 10.7266/N7416V0M
- 595 Poje, A. C., Özgökmen, T. M., Lippardt Jr., B. L., Haus, B. K., Ryan, E. H., Haza,
 596 A. C., ... Mariano, A. J. (2014). Submesoscale dispersion in the vicinity of the
 597 Deepwater Horizon spill. *Proc. Natl. Acad. Sci. U.S.A.*, 111(35), 12693–12698.
 598 doi: 10.1073/pnas.1402452111
- 599 Pumir, A., Shraiman, B. I., & Chertkov, M. (2000). Geometry of Lagrangian dis-

- 600 dispersion in turbulence. *Phys. Rev. Lett.*, *85*(25), 5324–5327. doi: 10.1103/
 601 PhysRevLett.85.5324
- 602 Romero, L., Uchiyama, Y., Ohlmann, J. C., McWilliams, J. C., & Siegel, D. A.
 603 (2013, September). Simulations of nearshore particle-pair dispersion
 604 in Southern California. *J. Phys. Oceanogr.*, *43*(9), 1862–1879. doi:
 605 10.1175/JPO-D-13-011.1
- 606 Schroeder, K., Chiggiato, J., Haza, A. C., Griffa, A., Özgökmen, T. M., Zanasca,
 607 P., ... Trees, C. (2012). Targeted Lagrangian sampling of submesoscale dis-
 608 perssion at a coastal frontal zone. *Geophys. Res. Lett.*, *39*(11), L11608. doi:
 609 10.1029/2012GL051879
- 610 Schroeder, K., Haza, A. C., Griffa, A., Özgökmen, T. M., Poulain, P. M., Gerin,
 611 R., ... Rixen, M. (2011). Relative dispersion in the Liguro-Provençal basin:
 612 From sub-mesoscale to mesoscale. *Deep-Sea Res Pt I*, *58*(3), 209–228. doi:
 613 10.1016/j.dsr.2010.11.004
- 614 Shulman, I., Penta, B., Richman, J., Jacobs, G. A., Anderson, S., & Sakalaukus,
 615 P. (2015). Impact of submesoscale processes on dynamics of phyto-
 616 plankton filaments. *J. Geophys. Res. Oceans*, *120*(3), 2050–2062. doi:
 617 10.1002/2014JC010326
- 618 Spydell, M. S., Feddersen, F., & Suanda, S. (2019). Inhomogeneous turbulent dis-
 619 perssion across the nearshore induced by surfzone eddies. *J. Phys. Oceanogr.*,
 620 *49*(4), 1015–1034. doi: 10.1175/JPO-D-18-0102.1
- 621 Torsvik, T., & Kalda, J. (2014). Analysis of surface current properties in the
 622 Gulf of Finland using data from surface drifters. In *Measuring and Mod-
 623eling of Multi-Scale Interactions in the Marine Environment - IEEE/OES
 624 Baltic International Symposium 2014, BALTIC 2014* (pp. 1–9). IEEE. doi:
 625 10.1109/BALTIC.2014.6887845
- 626 Yaremchuk, M., & Coelho, E. F. (2015). Filtering drifter trajectories sampled at
 627 submesoscale resolution. *IEEE J. Oceanic Eng.*, *40*(3), 497–505. doi: 10.1109/
 628 JOE.2014.2353472
- 629 Zavala Sansón, L., Pérez-Brunius, P., & Sheinbaum, J. (2017). Surface relative dis-
 630 perssion in the southwestern Gulf of Mexico. *J. Phys. Oceanogr.*, *47*(2), 387–
 631 403. doi: 10.1175/JPO-D-16-0105.1
- 632 Zhang, H.-M., Prater, M. D., & Rossby, T. (2001). Isopycnal Lagrangian statistics

633

634

from the North Atlantic Current RAFOS float observations. *J. Geophys. Res.*,
106(C7), 13817–13836. doi: 10.1029/1999JC000101

Accepted Article